The HERA-B Ring Imaging Čerenkov Counter

I. Ariño [b] J. Bastos [c] D. Broemmelsiek [d] J. Carvalho [c] P. Conde [b] D. Dujmić [a] R. Eckmann [a] L. Garrido [b] A. Gorišek [i] I. Ivaniouchenkov [c] M. Ispirian [f] S. Karabekian [e] S. Korpar [k,i] P. Križan [j,i] S. Kupper [g,i] K. Lau [f] R. Miquel [b] D. Peralta [b] R. Pestotnik [i] J. Pyrlik [f] D. Ramachandran [f] K. Reeves [a] J. Rosen [d] R.F. Schwitters [a] M. Starič [i] A. Stanovnik [h,i] D. Škrk [i] T. Živko [i]

[a] *University of Texas, Austin, USA*

[b] *University of Barcelona, Spain*

[c] *LIP Coimbra, Portugal*

[d] *Northwestern University, Evanston, USA*

[e] *DESY, Hamburg, Germany*

[f] *University of Houston, Houston, USA*

[g] *Slovenian Research Institute, Klagenfurt, Austria*

[h] *Faculty of Electrical Engineering, University of Ljubljana, Slovenia*

[i] *J. Stefan Institute, Ljubljana, Slovenia*

[j] *Faculty of Mathematics and Physics, University of Ljubljana, Slovenia*

[k] *Faculty of Chemistry and Chemical Engineering, University of Maribor, Slovenia*

Abstract

The HERA-B RICH uses C_4F_{10} as radiator gas and a large 24 m^2 spherical mirror for imaging. The photon detector employs 2240 Hamamatsu multi-anode photomultipliers with a total of 27,000 channels. To match the anode dimension to the dispersion error and to solve the PMT packing problem we used a 2:1 reducing two-lens telescope in front of each PMT.

The design performance of the RICH was fully reached: the average number of photons for a $\beta = 1$ particle detected in the RICH was found to be 32; a single hit resolution of 0.7 mrad was reached.

The counter has been completed in January of 1999, and its performance has been steady and reliable over the years it is in operation.

Preprint submitted to Elsevier Preprint *15 January 2002*

Key words: ring imaging Cherenkov detectors, photomultiplier tubes, HERA-B

1 Introduction

The HERA-B experiment (1) was designed to measure rare processes in the decays of B mesons. The B mesons are produced in collisions of 920 GeV/c protons with a fixed target. The target consists of 8 wires in the halo of the proton beam in order not to disturb experiments measuring ep collisions. One of the essential components of the spectrometer is the ring imaging counter (RICH) (1; 3; 4). The main purpose of the RICH counter is the identification of charged hadrons, in particular kaons, into which the B meson decayed. Identifying the charged kaon essentially means separating it from the pion between 3 GeV/c and about 50 Gev/c at an interaction rate of up to 40 MHz. In what follows we shall describe the essential components of the counter, and will then present the results of the commissioning phase.

2 Design criteria

to be added

3 Realization

3.1 Radiator

Perfluorobutane gas (C_4F_{10}) has been chosen for the HERA-B RICH radiator, since it combines a relatively high refractive index, $n = 1 + 1.35 \times 10^{-3}$, and low dispersion, 5% variation in $n - 1$ (?) in our spectral acceptance from 300 to 480 nm. In this gas the Čerenkov radiation threshold momenta for pions and kaons are at 2.7 GeV/c and 9.6 GeV/c, respectively. For $\beta = 1$ particles,

the Čerenkov angle is 52 mrad, while the $\pi - \mathrm{K}$ difference in Čerenkov angle is 0.9 mrad at 50 GeV/c. The angular spread due to dispersion amounts to 0.5 mrad (?) r.m.s. Since some of the freons are know to scintillate considerably, as e.g. CF_4, we have checked in a study (32) during an early design phase that the scintillation background should be negligible.

The radiator vessel made from stainless steel plates with 1 mm aluminum particle entrance and exit windows is placed about 11 m downstream of the target (see Figure 1). Two beam shrouds made of capton-reinforced plastic (?) close the gas volume around the two beam pipes for protons and electrons. Light exits the vessel through 2 mm thick UV grade Plexiglas windows. The vessel is filled with 108 m^3 of C_4F_{10} gas, which is being circulated in a closed system with liquification stages for cleaning and buffering (5) (or Appendix?). Requirements on impurities are moderate due to the operating range in the near UV and the visible part of the light spectrum.

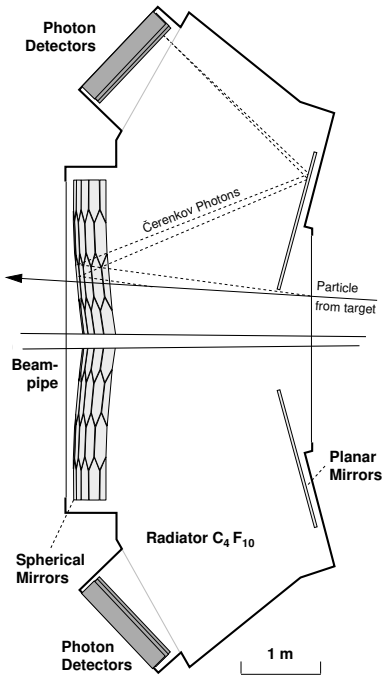

Fig. 1. Schematic of the RICH. Rays emitted by a particle and their path to the photon detector are indicated.

3.2 Mirrors

The main imaging device is a spherical mirror, placed inside the radiator with the center of the sphere near the target and a radius of curvature of 11.4 m. The mirror, a 6 m by 4 m rectangular cutout from the sphere, is made up of 80 full or partial 7 mm thick hexagons made from Pyrex glass, coated with 200 nm aluminum and 30 nm MgF_2 (see Fig. 2). To be able to place the focal

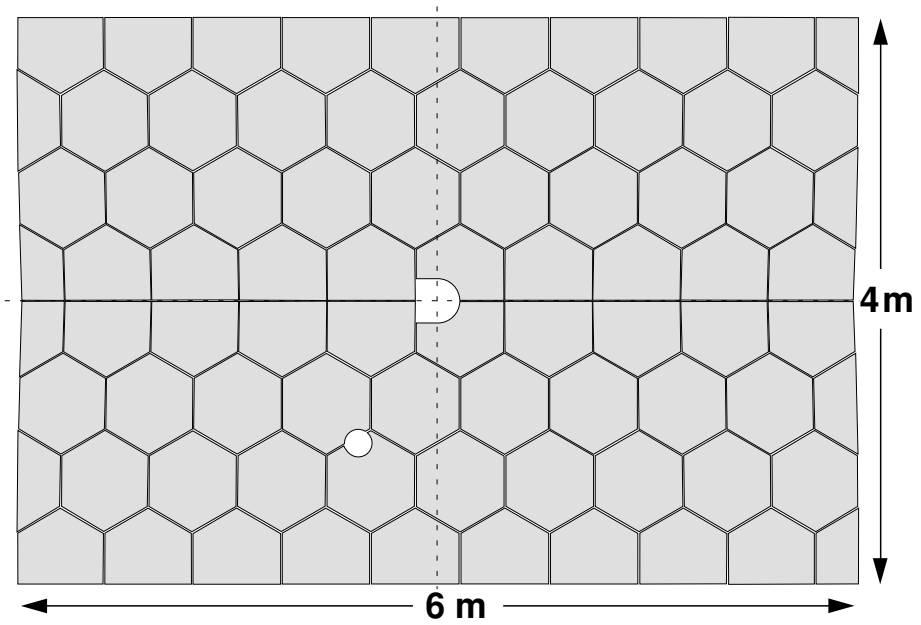

Fig. 2. Distribution of spherical mirror multigons. The holes in the center are for the proton and electron beam pipe.

surface outside of the particle flux (±160 mrad vertically), the mirror is split horizontally and both halves are tilted by 9° away from the beam-line. A set of two planar mirrors, composed of 18 rectangular elements each, translates the focal surface conveniently to an area above and below the radiator vessel (see Fig. 1). All 80 spherical as well as the 36 planar mirrors are mounted on a rigid low mass support structure inside the radiator volume and can be individually adjusted by stepper motors from the outside.

The mirror quality has been determined upon delivery by measuring for each segment the radius of curvature, and the fraction of reflected light, as well as by recording a Ronchi image to check the homogeneity of the mirror surface. The reflectivity was required to exceed 85% in the wavelength interval 250 nm - 600 nm. The planar mirrors are made of float glass, thus being significantly cheaper at the required optical quality. By making use of the data gathered on all the mirror segments, it was possible to group them in the tiling scheme according to their optical quality and resolution requirements (6).

All mirrors have been aligned to better than the needed precision by surveying them inside the vessel. An additional off-line data based alignment algorithm of the mirror segments has been developed (7).

3.3 Photon detector

Initially, two wire chamber based photon detectors were considered, a CsI photocathode in a MWPC and a TMAE based detector with 10 cm deep, 8 x 8 mm^2 unit cells. After considerable success of on-the-bench and beam tests (8; 9; 10), the detectors were tested in a high rate environment as expected in the HERA-B experiment. Both wire chamber based detectors had to be abandoned; the TMAE detector showed a prohibitive decrease of avalanche gain due to aging effects (11; 12), while the CsI photocathode could not be routinely produced and maintained with sufficiently high quantum efficiency in addition to problems with rates in excess of a few kHz per pixel (13; 14).

The final photon detector consists of Hamamatsu multianode R5900 M16 and M4 photomultiplier tubes. The M16 version has 16 pads of 4.5 x 4.5 mm^2 each, with a 12-stage, metal-foil dynode system (15). The M4 version has 4 pads of 9 x 9 mm^2 each, and 10 dynodes. The quantum efficiency of the photocathode with borosilicate window has a broad plateau in the wavelength region between 300 nm and 500 nm with a maximum value of 20%. The UV-extended version has a UV transparent window, which shifts the low wavelength cut-off to about 250 nm. The other PM characteristics such as the required cathode high voltage ($\leq$ 1000 V), the current amplification (10^7), dark current ($\sim$ 1 nA), pulse rise time (0.8 ns), transit time spread (0.3 ns) (15), are also satisfactory.

In the initial set of on-the-bench measurements (25) the single photon counting properties of the photomultiplier tube were investigated, in particular the efficiency for single photon detection as well as the background count rate. It was established that the tube allows for a good single photoelectron detection, with good uniformity (Fig. 3), very little cross talk and low background count rate.

Tests of all the 2305 acquired PMT's (1543 M16's and 762 M4's) have been made in the laboratory prior to the installation in the photon detector (30). Čerenkov photons produced by β electrons of a ^{90}Sr source were used as a stable light source. Four tubes were tested at the same time, of which one was used as a reference. For each photomultiplier tube, the source and background rates were recorded as a function of high voltage and threshold setting. On the basis of these tests, the photomultipliers have been grouped according to similar high voltage characteristics, allowing all PMT's within a group to be connected to the same high voltage, thus maximizing the efficiency for the given, much smaller number of independent HV channels (24). The results obtained for the optimal high voltage as well as for the relative PMT sensitivity were compared to values provided by the manufacturer, and a good agreement was found (30). The count rates of the reference M4 and M16 photomultipliers

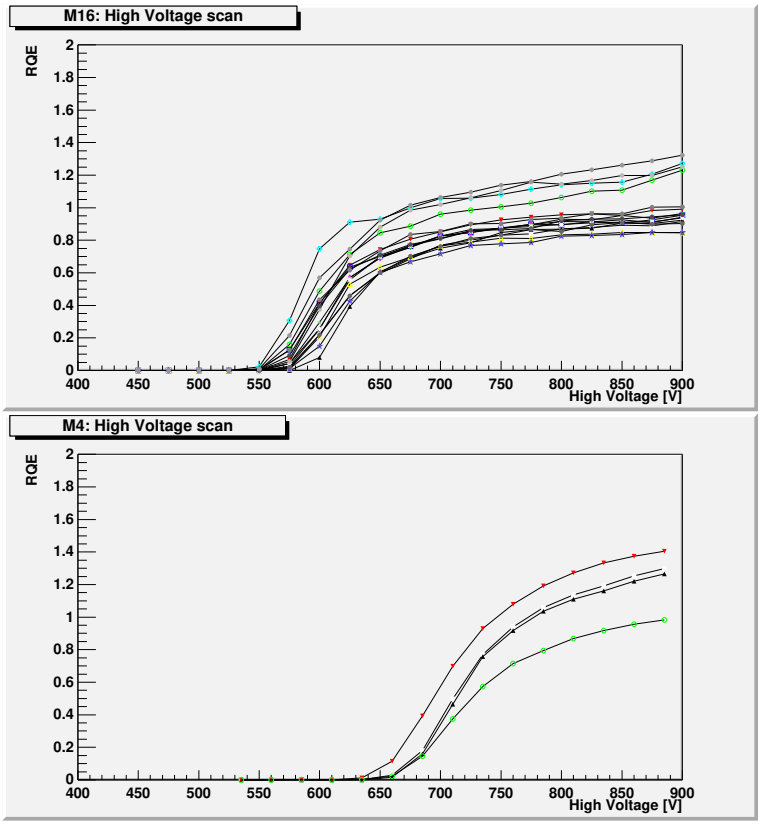

Fig. 3. Dependence of a suitably normalized rate as a function of the high voltage for all channels of a representative M16 (above) and M4 (below) photomultiplier tube.

were recorded during the quality assessment tests, and were also continually measured after the tests were finished, in order to obtain an estimate of the long term stability. The count rate decrease in two years is consistent with the known decay rate of the ^{90}Sr source.

The outer dimensions of the PMT are 28 x 28 mm^2, so the photocathode occupies only about 30% of the surface. Due to the smaller photocathode surface compared to the photomultiplier cross section, a two lens demagnification system (2:1) was designed (Fig. 4) (16). The lenses are made of UVT perspex with high transparency over most of the wavelength region where the photocathode is sensitive (Fig. 5). The angular acceptance of the optical system is also satisfactory and is uniform for incident angles below about 110 mrad (17). In addition to increasing the active area the lens system also adjusts the required pixel size in the central detector region (9 x 9 mm^2) to the PMT pad size 4.5 x 4.5 mm^2. The resulting angular measurement error (0.5 mrad) matches the spread due to dispersion (0.45 mrad)???. The outer detector region with lower occupancy and looser resolution requirements uses the M4 version of the tube with two times larger pads (9 x 9 mm^2) with the same lens system, such that the pixel size amounts to 18 x 18 mm^2.

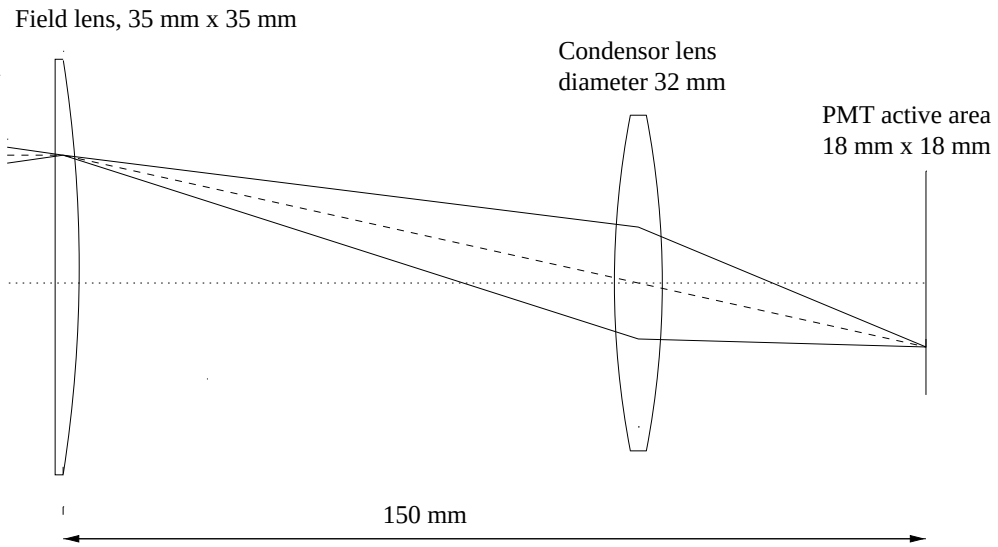

Fig. 4. The optical system for light collection and demagnification. The two rays shown in full line correspond to photons with incident angles of ±100 mrad.

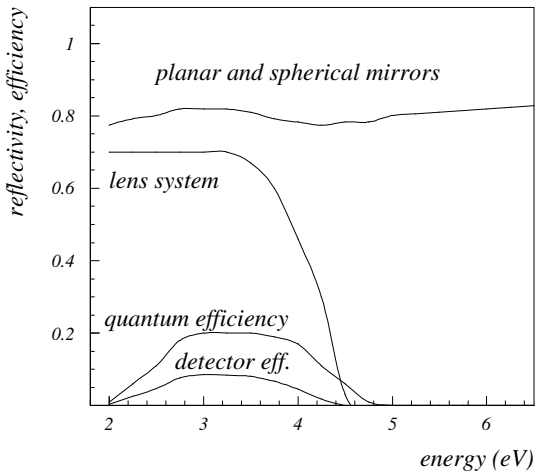

Fig. 5. Transmission of the lens system, reflectivities of the mirrors and quantum efficiency of the photomultiplier tubes.

In order to reduce the contribution of spherical aberration to the overall resolution of the Čerenkov angle, an optimal surface of the Čerenkov photon detector has been calculated (22; 23). Each half-detector (upper and lower) consists of 5 flat supermodules placed in order to approximate the optimal surface, which is close to the shape of a flattened (ellipsoidal) cylinder. Such an arrangement also ensures better acceptance for the Čerenkov photons, which should be incident onto the flat supermodules at angles below 110 mrad. The supermodules are rectangular 1.1×0.4 m^2 boxes containing a grid made from 1 mm thick soft iron sheet that serves as magnetic shield and mounting structure for the base-boards and the light collection system. The two types of photomultipliers have been arranged according to occupancy and reconstruction requirements

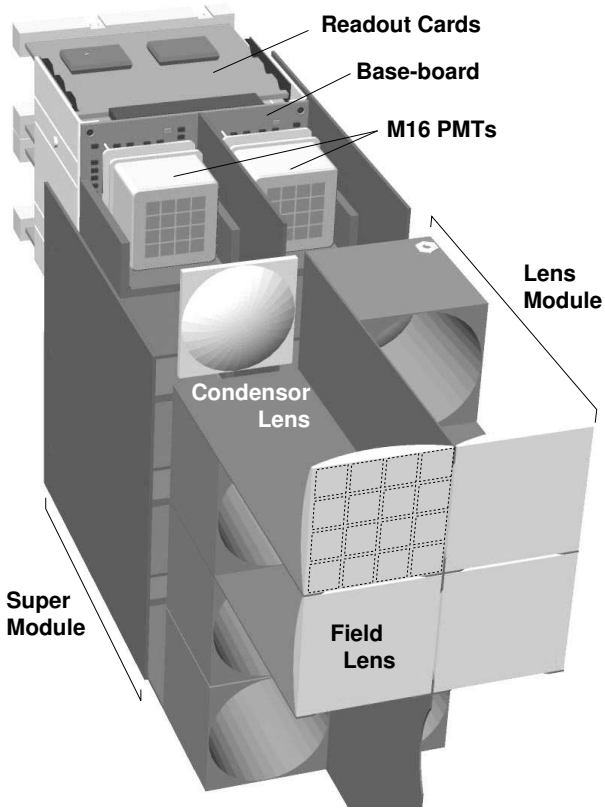

Fig. 6. Schematic of the RICH photon detector.

as indicated in Fig. 7.

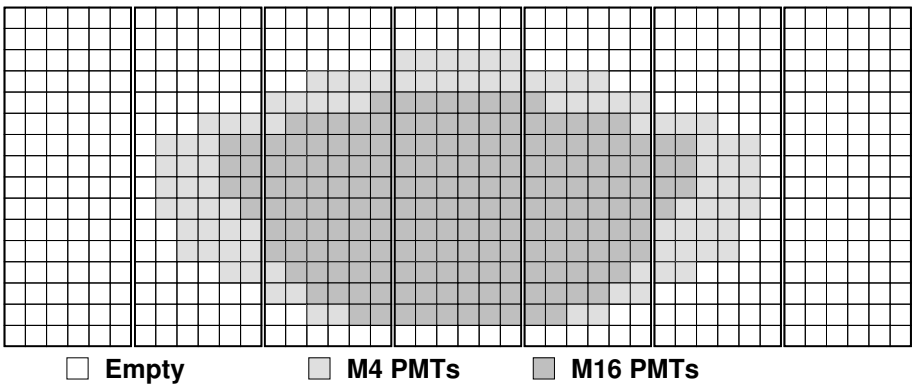

Fig. 7. Arrangement of M4 and M16 type basic units on the 7 supermodules of the upper focal plane.

3.4 Read-out and monitoring

To mount, power, and read out the photomultipliers we have developed two types of base-boards, one for M4 and one for M16 PMTs. Each base-board is

a light tight four-layer FR4 circuit-card, 70 $\times$ 70 mm^2 in size, equipped with surface mount components. The board holds four custom designed sockets and divider chains, appropriate for the type of PMT, on one side; the other side contains one (M4) or four (M16) connectors for the 16-channel readout-cards, attenuation circuitry and two daisy-chainable high voltage connectors. The base-boards are mounted in such a way, that all PMTs are positioned on 36 mm centers (see Fig. 6). In Fig. 8 a photograph of a fully equipped basic module for the M16 photomultiplier tubes is presented.

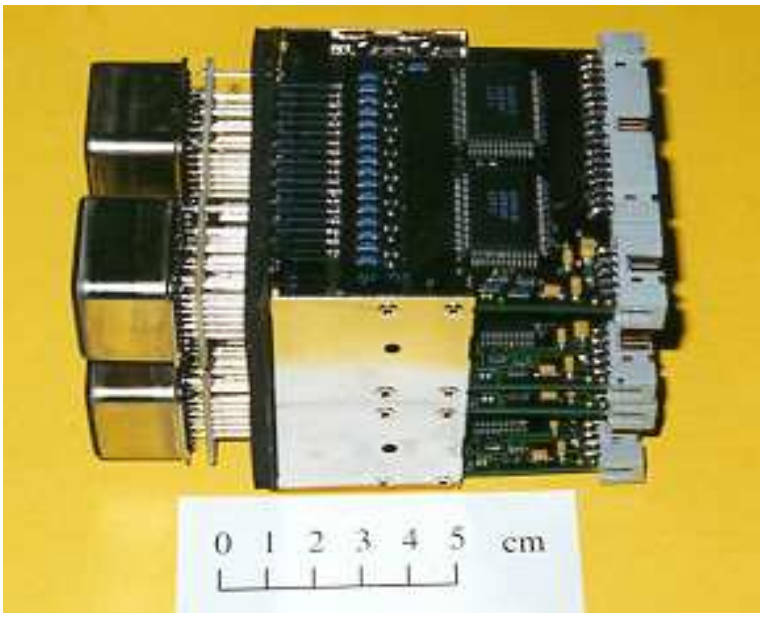

Fig. 8. Fully equipped photomultiplier basic module housing Hamamatsu R5900 photomultiplier tubes type M16.

The bleeder chain was optimized by varying the composition of the 13 resistors (27). Very little dependence of rate at the high voltage plateau was seen when varying the fraction of 1 MΩ to 560 kΩ resistors. Somewhat better results were obtained with the first three steps of 1 MΩ resistors, followed by ten 560 kΩ resistors. This bleeder chain was then adopted for the M16 photomultiplier tube. For the M4 photomultiplier a similar voltage divider was chosen, where again the first three resistors had twice the value of the other eight.

Between two and five base-boards, with their PMTs selected for similar optimal operating voltage (range 750 to 890 V), are powered by a single output from a 160-channel CAEN SY527 high-voltage supply (24).

The front end electronics board employed in the system is a 16-channel board based on the ASD8 (18), an amplifier, shaper and discriminator chip. The board (19) has been developed for the Outer Tracker (OTR), the main tracking system of the HERA-B experiment. The front end electronics boards were arranged according to their optimal threshold voltage, by using test data.

Two types of tests were performed (28), one looking at the response of all the channels using the test pulse, and the other surveying the response of each channel. Both tests were repeated for different heights of the pulses and different values of threshold voltages.

The low voltage supply system for the ASD8 boards is powered by four KEPCO ATE 6-100DM supplies, delivering the voltages of + 3 V and − 3 V to the upper and lower photon detector half separately. For diagnostic purposes analog outputs of 20 photon detector channels are led to the electronics hut.

Digital outputs of the front end electronics boards are connected via 7.5 m long 34 wire twisted flat cables to the front end driver system. The front end driver system is composed of front end driver crates which accept front end driver daughter-boards and mother-boards. The front end driver daughter board accepts 16 signal cables and thus supports 256 channels. The input data is stored in an input buffer with 128 locations at the bunch crossing period of 96 ns until the first level trigger indicates an event of interest. The front end driver mother board is designed as a control and transmitter unit for event detection application. It reads the channels of four front end daughter boards. The implemented high speed SHARC (20) link interface then transmits the data from all channels to a host SHARC processor system. Since a front end driver crate houses eight daughter-boards and two mother-boards, 14 crates are neded for reading out of 1676 flat signal cables.

A sizable fraction of the operating parameters of the RICH counter (low voltage and threshold for the front end electronics boards, the temperatures at the photon detector and at the power supplies) are controlled by a Field Point (29) based system. Two separate systems are used for monitoring of the high voltage (CAEN?) and steering of the gas system (5). The overall control of these systems is realized with a cover program...

As a triggerable light source for testing of the photon detector in the periods without beam induced reactions, a system of light emitting diodes (LED) was installed at the sides of the photon detector windows (21). The system provides good illumination over the whole photon detector area.

3.5 Analysis tools

Several tools were developed for the analysis and monitoring of the data collected by the RICH counter. In the initial phase of the commissioning of the HERA-B experiment when major parts of the main tracking system were not yet available, a stand-alone ring search algorithm was employed (34). With it RICH could be used as a tracking device as described in section ... The algo-

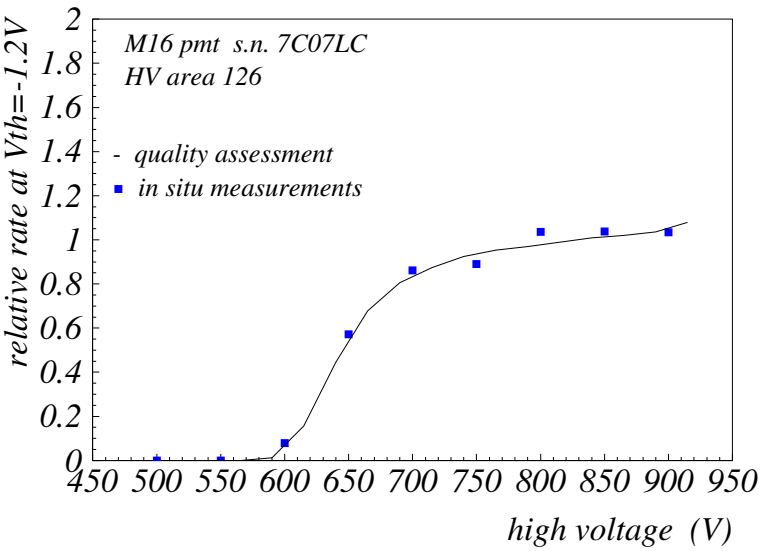

Fig. 9. The plateau curve for a typical M16 tube. The data labeled 'in situ' represent values measured during the photon detector testing in its final position, while the curves labeled 'quality assessment' correspond to measurements made in the laboratory during on-the-bench quality tests. The two sets of data are normalized to the average of the three points at 750 V, 800 V and 850 V.

rithm is routinely used to monitor the maximum value of the Čerenkov angle (35) which is, in turn, used as the input for particle identification algorithms. We note that several versions of the ring search algorithms were successfully tried on the data (36).

For highly populated events, typical for the reactions as recorded in the HERA-B spectrometer, additional information is required. The main tracking system should provide track directions (resulting in ring center) and track momentum (allowing only Cherenkov angles corresponding to the expected particles). Accurate knowledge of the signal and background shapes and very precise measurements of the Cherenkov angle with good track resolutions will all contribute to the improvement of particle identification. In this case, extended maximum likelihood methods were applied, either directly (37; 39) or combined with an expectation-maximization algorithm (38). The later is used as the main particle identification method, and is described in more detail in section ...

4 Measurements and results

4.1 Test measurements in situ

With the photon detectors in their proper position in the HERA-B spectrometer, the photomultipliers cabled to the readout system and with freon as Čerenkov radiator, the commissioning of the system became possible. Fig. 9 gives the count rate versus high voltage for a representative photomultiplier. It is seen that the curves measured in-situ with the HERA proton beam agree nicely with the ^{90}Sr source measurements. The occupancy is shown in Fig. 10, where the region occupied by M16 PMT's is clearly distinguished from the region occupied by M4 PMT's. We also note that only about 0.3% of the nearly 30.000 channels were found to be noisy, and were excluded from further analysis. As a result, very clean rings can be observed in low multiplicity events such as the one shown in Fig. 11. The absence of random hits in the event also confirms the earlier result that the background due to scintillation in the radiator gas is negligible.

4.2 Basic RICH parameters

From the data available on the quantum efficiency (15), mirror reflectivities (6), window and optical system transmissions (16), one calculates the merit factor $N_0 = 43$ cm^{-1}, such that the expected number of photons for particles approaching the velocity of light amounts to $N_{det} = N_0 L \sin^2\vartheta = 32$ with $L =$ 2.75 m and $\vartheta = 52$ mrad. The expected single photon resolution is 0.7 mrad and 1 mrad for the regions occupied by M16 and M4 PMT's, respectively, and is based on known dispersion of C_4F_{10}, detector granulation and optical errors.

4.3 Number of photons

In order to obtain the basic RICH parameters from the data, we have initially analyzed only events with a small number of Cherenkov rings (Fig. 12). For each ring, the number of photon hits was counted and the Cherenkov angle was determined obtaining a point in Fig. 2. It is seen that most of the rings fall within a one sigma deviation from the expected dependence of the number of photons versus the Cherenkov angle. The largest measured Cherenkov angle of 52 mrad also corresponds to the expectation for $\beta = 1$ particles ($cos\theta_c = 1/n$), for which the average number of detected photons is 32 per ring. The number of detected photons on a ring measured by a Cherenkov detector is often

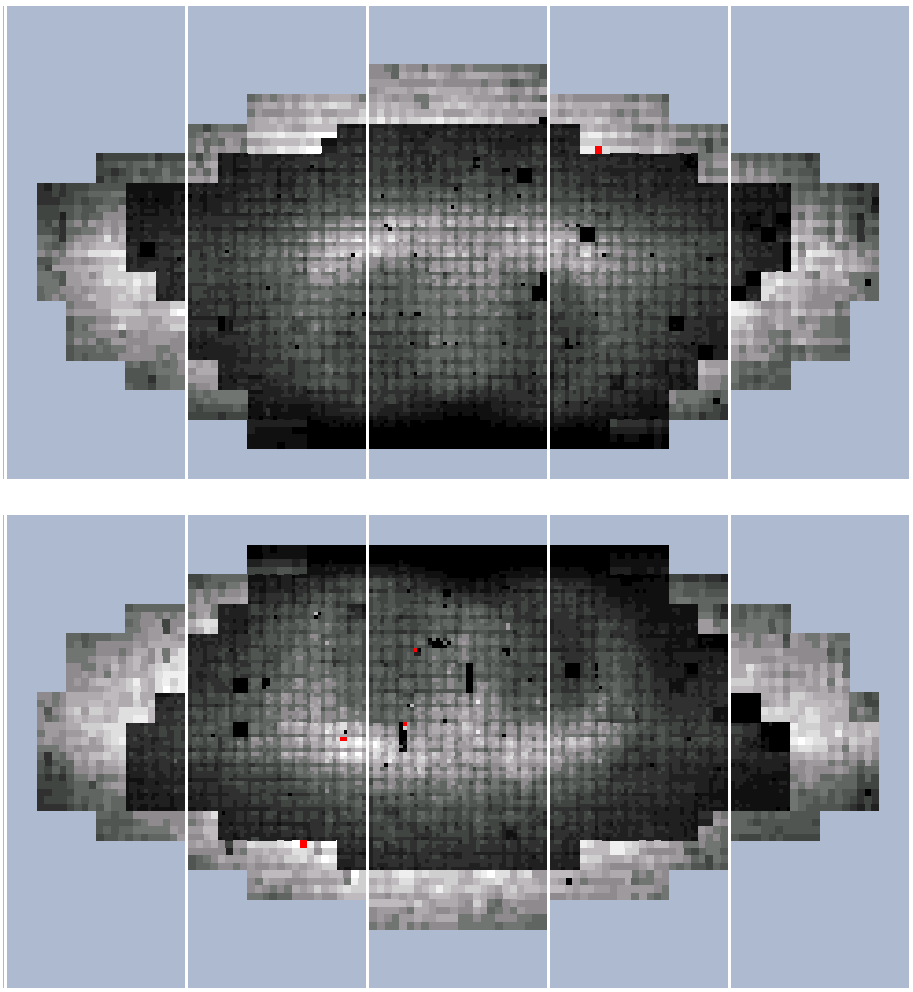

Fig. 10. The occupancy of the upper and lower photon detectors shows the region occupied by M16 (inner region) and M4 PMT's (outer region). The peak values, shown in white, correspond to rates around 1.5 MHz per channel.

parametrised as $N = N_0 L sin^2\theta_c$, where L is the length of the radiator and N_0 is the detector response parameter. This parameter was calculated for 184 isolated rings and the distribution is plotted in Fig. 13, from which it is seen that the mean value is 43 cm^{-1}.

4.4 Angular resolution

To determine the Cherenkov angle uncertainty given by a single Cherenkov photon, for each track one fills a histogram with the photon hits at their corresponding Cherenkov angle so the hits due to $\beta = 1$ rings should show up as a peak, as shown on Fig. 14 for M16 photomultiplier tubes. The distribution has been fitted with Gaussian peak and polynomial background. As expected, the single photon resolution depends on the particle momentum. Below 50 GeV it is mainly determined by the track angular uncertainty (Fig. 15), with a

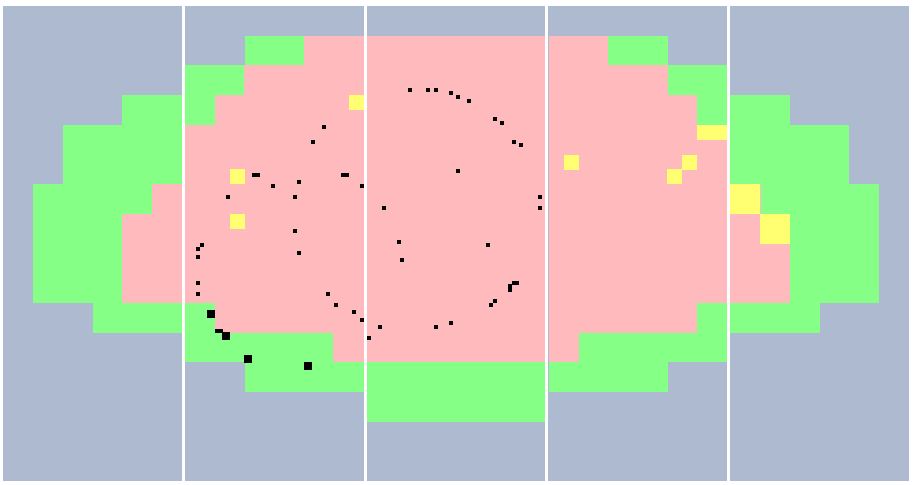

Fig. 11. Event with two Cherenkov rings on the lower photon detector.

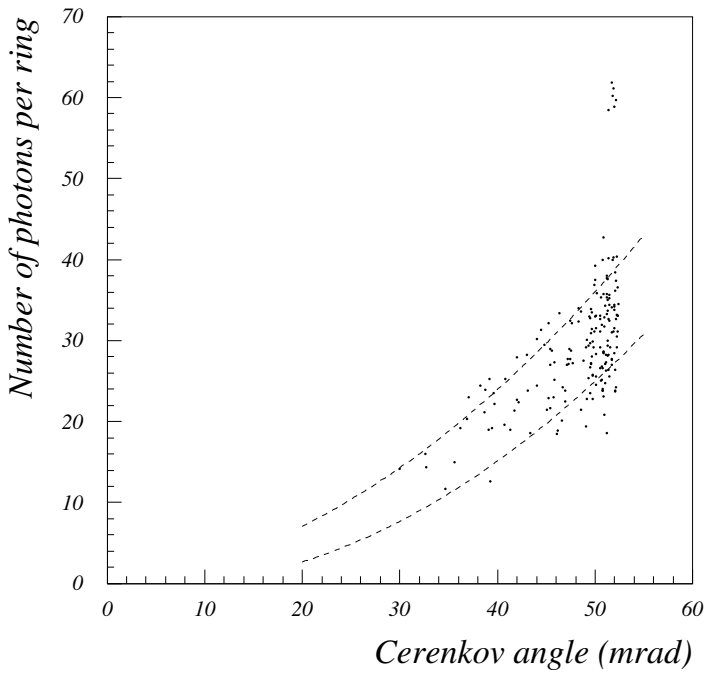

Fig. 12. Number of photons on a ring versus the corresponding Cherenkov angle. The points represent measurements of individual rings, while the dashed lines correspond to one sigma deviations from the predicted dependence. The small group of events at $\theta_c = 52$ mrad, which has about two times the number of photons per ring, probably corresponds to an overlapping e^+e^- pair.

mean value of 1.4 mrad. For the very well defined high momentum tracks the resolutions of 0.7 mrad for the M16 (9 mm x 9 mm pixel region) and 1.0 mrad for the M4 (18 mm x 18 mm pixel region) have been measured. These measured values agree nicely with estimates discussed above.

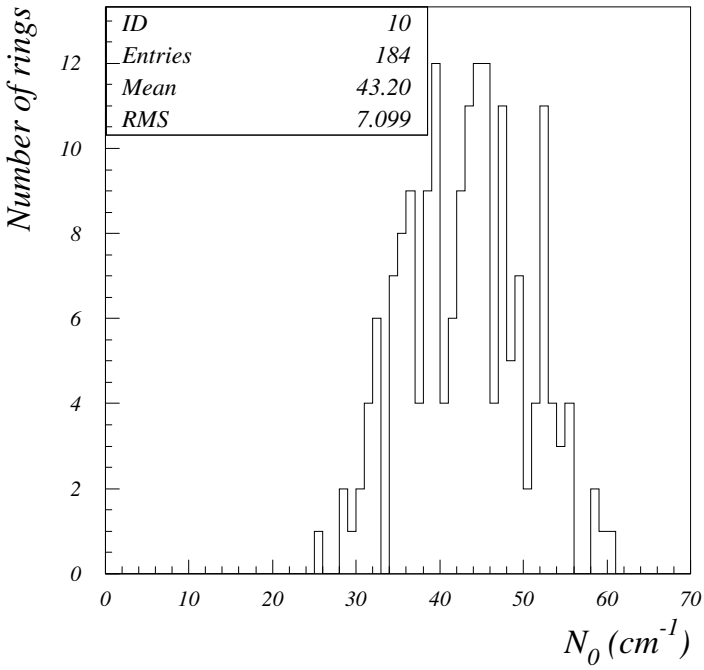

Fig. 13. Distribution of the RICH response parameter N_0.

The intrinsic resolution of the RICH counter was also checked by the stand-alone ring search analysis (40), and is consistent with the design values of 0.7 mrad and 1 mrad for M16 and M4 PMT's. The intrinsic resolution in Cherenkov angle given by a single Cherenkov photon has also been obtained with the aid of hits in the electromagnetic calorimeter (ECAL). The center of the Cherenkov ring is accurately determined from the straight line connecting the center of the ECAL cluster with the wire target (the magnetic field was off for this measurement). Note that the contribution of cluster spatial resolution to the peak width is negligible for the given set of tracks with cluster energy above 50 GeV. The single Cherenkov photon resolutions obtained correspond to $\sigma = 0.7$ mrad and $\sigma = 1.0$ mrad for the M16 and M4 PMT's respectively.

Besides the basic RICH parameters, the particle identification capabilities are affected also by the high multiplicity of rings in a single event. Typically 50 overlapping rings are present in the event of which about 1/3 could be associated with the measured tracks. In addition, channel occupancies in some regions are as large as 25%. ...

As an illustration of particle identification capabilities a likelihood fit was performed on Čerenkov angle distributions for individual tracks. Fig. 16 shows the resulting bands for different particles in the plot of reconstructed Čerenkov angle versus momentum as obtained by analyzing a sample of measured data. Kaons are clearly resolved from pions in the momentum range from pion

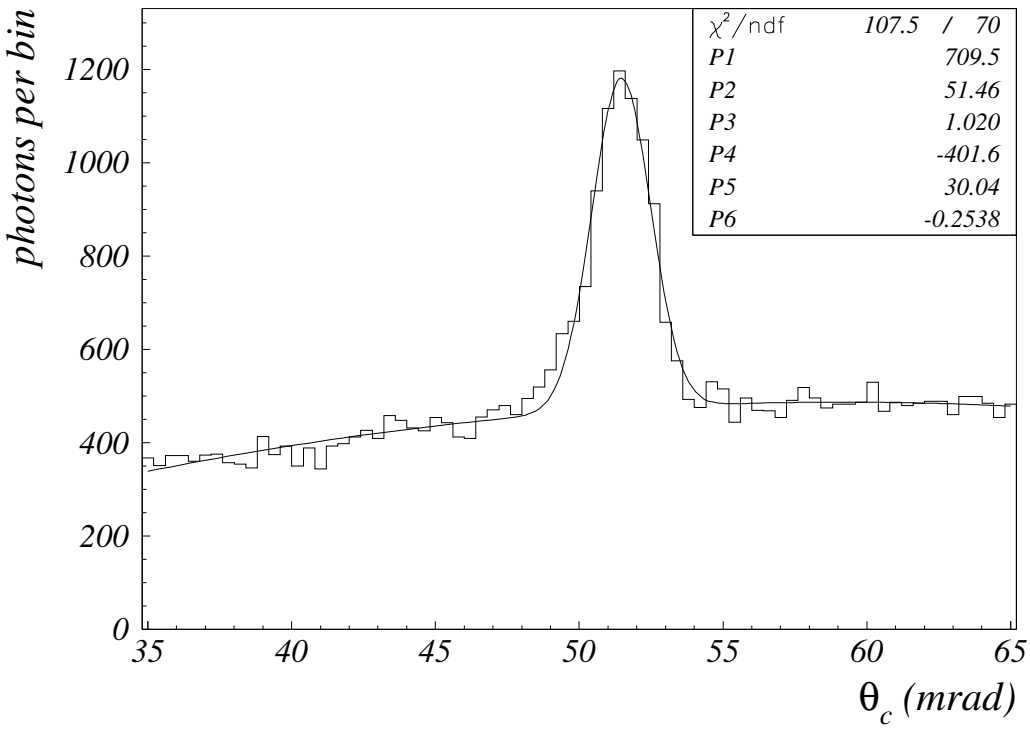

Fig. 14. Single photon resolution for M16 PMT's: distribution of the measured Čerenkov angle for individual hits in the case of tracks with momenta above 50 GeV/c

threshold to at least 40 GeV/c and similarly the protons in the momentum range up to 70 GeV/c or more. Also a separation of kaons from protons is possible in the range above the kaon threshold to approximately 70 GeV/c.

5 Particle identification performance

5.1 Method

For efficient particle identification of highly populated events, the main tracking system should provide track directions (resulting in ring center) and track momentum (allowing only Cherenkov angles corresponding to the expected particles). Accurate knowledge of the signal and background shapes and a precise measurements of the Cherenkov angle with good track resolutions will all contribute to a good particle identification.

For particle identification we use the extended likelihood method, combined with the expectation-maximization algorithm. The method is described in detail in Ref. (38). The first step in the method is the calculation of Čerenkov

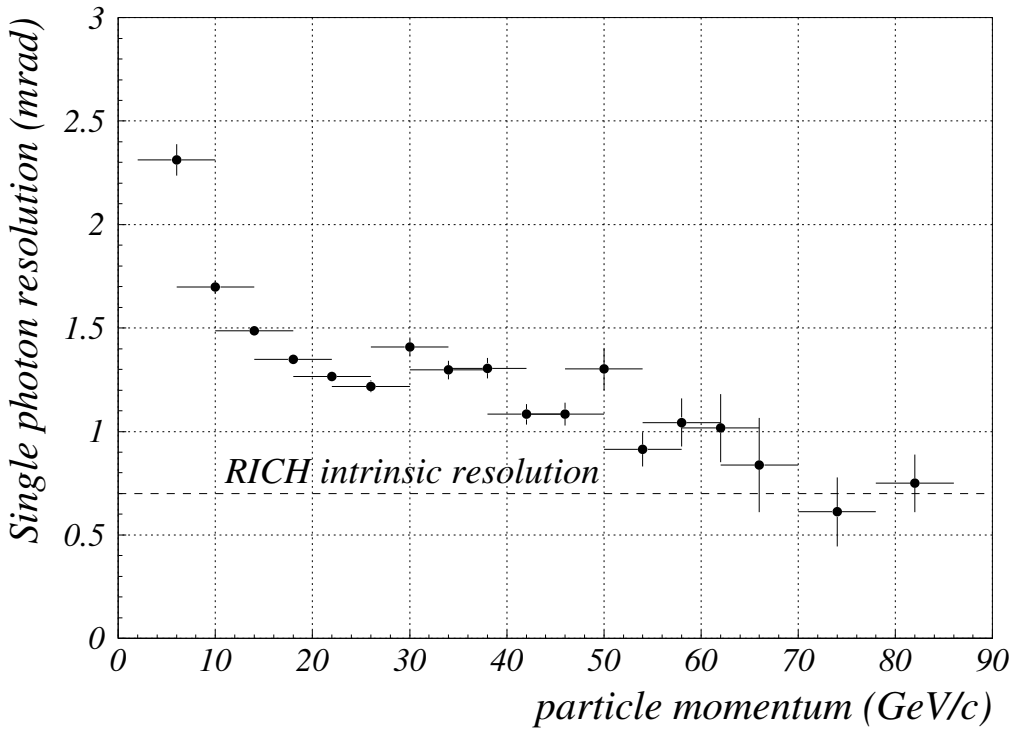

Fig. 15. The measured single photon Čerenkov angle resolution versus particle momentum for the region covered by M16 photomultiplier tubes.

angle (as described in Ref. (22)) for all track-photon pairs with the Čerenkov angle smaller than 70 mrad. The Čerenkov angles of the pairs are stored in a list, together with a probability (weight, w_i) that the photon from a pair is emitted by the track of that pair. Initially the weights are set to $1/N_{track}$, where N_{track} is the number of tracks corresponding to a specific photon hit. In the next step the expectation-maximization algorithm is applied to the list of pairs. The result of the algorithm is a set of new values of weights w_i. In this way the track-photon pair which is more likely to be the right one, gets a larger weight.

In the last step the extended likelihood probabilities are calculated for 6 possible hypothesis for the identity of a track: *electron*, *muon*, *pion*, *kaon*, *proton* and *other*. The last one represents the case, when the distribution of Čerenkov angles of photons for a given track is consistent with the background. The resulting likelihood probabilities have the range of values between 0 and 1 and are normalized so their sum equal to one.

The selection of tracks belonging to a particular particle type is made by applying a cut on the appropriate likelihood. For easier use we defined three levels of selection: *soft*, *medium* and *hard*. The levels are set to 0.05 (*soft*), 0.50 (*medium*) and 0.95 (*hard*) for pion selection and 0.05 (*soft*), 0.30 (*medium*) and 0.95 (*hard*) for kaon or proton selection.

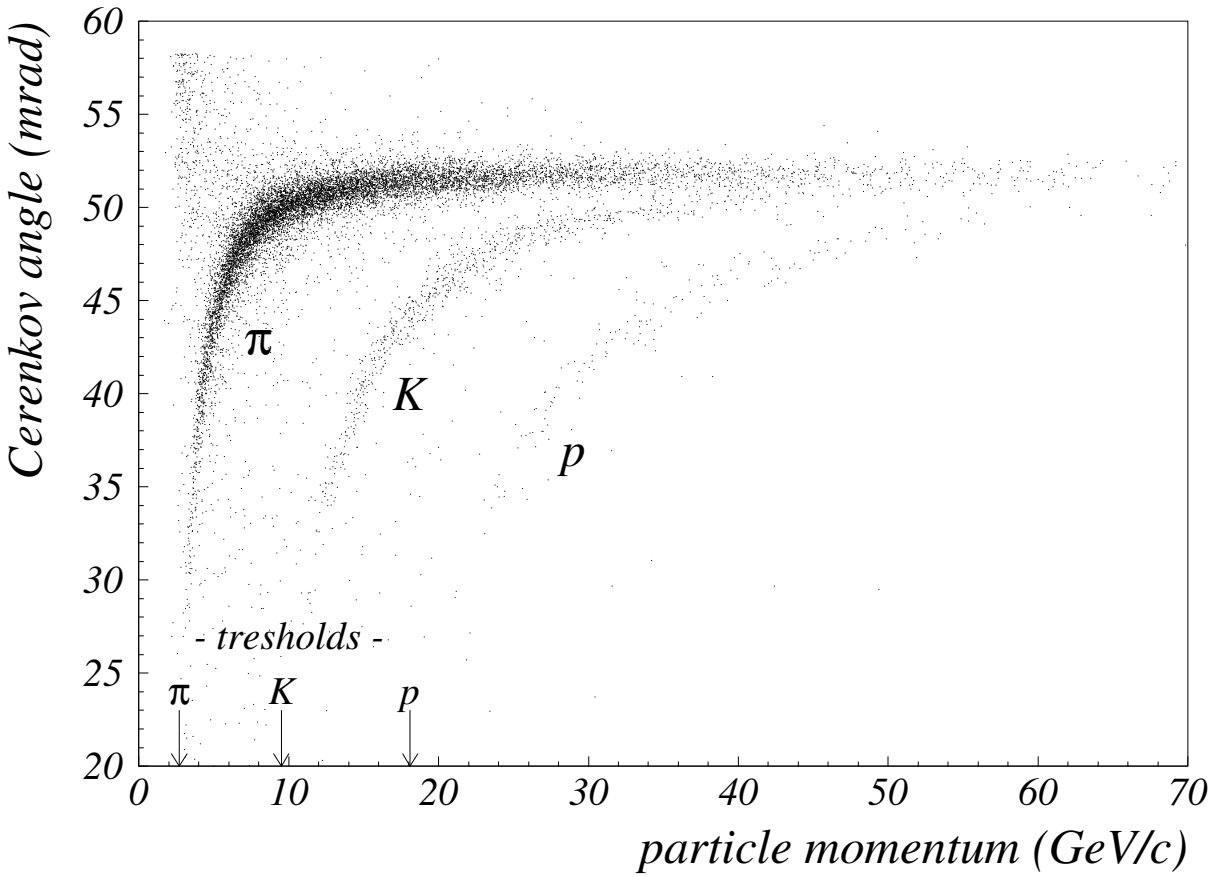

Fig. 16. Reconstructed Čerenkov angle versus particle momentum. Bands for pions, kaons and protons are clearly visible.

5.2 Results

To evaluate the efficiencies and mis-identification probabilities on the real data an apriori knowledge of particle types is required. The following reconstructed decays have been used: (1) $K_s \to \pi^+\pi^-$, as a source of pions, (2) $\Lambda \to p\pi^-$ and $\bar{\Lambda} \to \bar{p}\pi^+$, as a source of protons, anti protons and pions, and (3) $\phi(1020) \to K^+K^-$, as a source of kaons.

For the first two decays a very clear signal in the invariant mass plot is obtained by cutting on the secondary vertex distance and removing the reflections (Λ, $\bar{\Lambda}$ in K_s and vice versa). The last one comes from the primary vertex together with roughly 10 other particles. Invariant mass plot shows a huge combinatorial background. To lower the background, one of the particles has been used to tag the decay by identifying it as a kaon and applying a transverse momentum cut. The other one has been used for efficiency and mis-identification evaluation.

In all cases the number of particles of a given type surviving the selection criteria and the number of all particles of the same type in a selected momentum bin have been obtained by fitting a Gaussian plus linear function to the invariant mass plots.

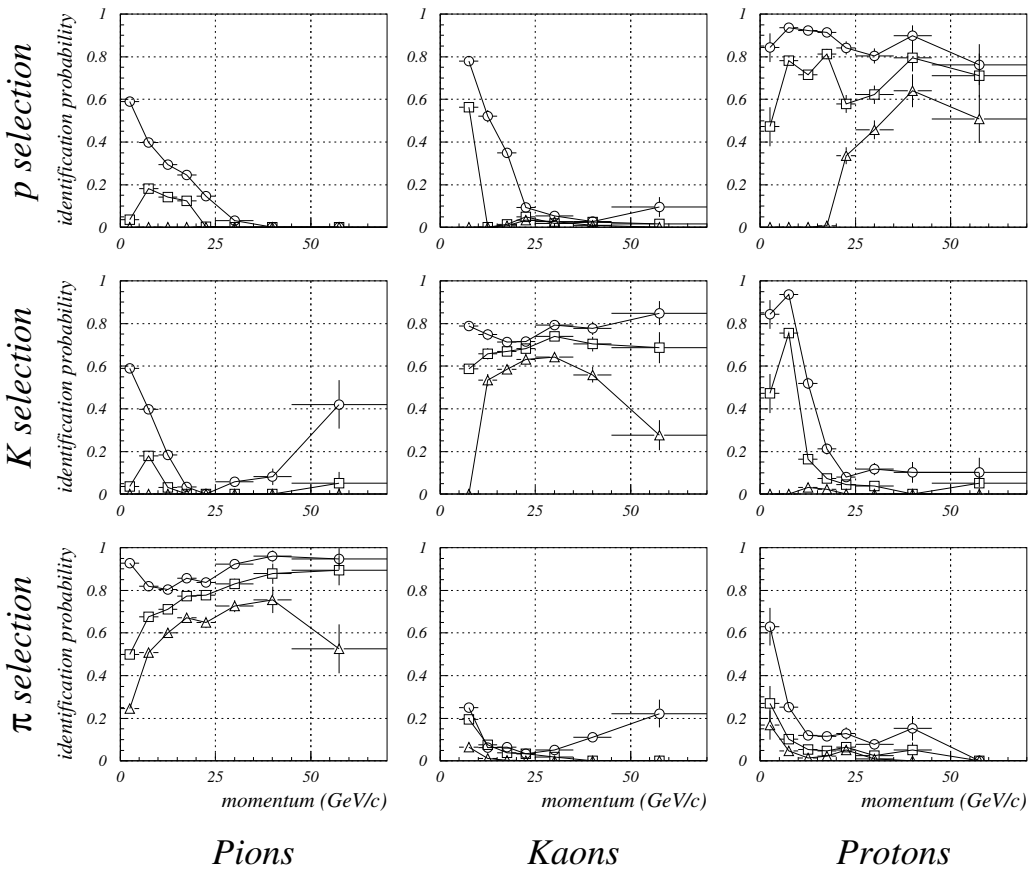

Fig. 17. Momentum dependent identification probability plots for soft (circles), medium (squares) and hard (triangles) selections. Plots on the diagonal show the efficiency, plots left or right to diagonal show the mis-identification probability.

The results are presented in Fig.17. At medium selection criteria a 65% to 75% kaon identification with less than 4% pion mis-identification probability is achieved between 10 and 70 GeV/c, and 60% to 80% proton identification with less than 1% pion mis-identification probability is achieved between 20 and 70 GeV/c. Below Čerenkov threshold the efficiencies are 60% for kaons (5 - 10 GeV/c) with 18% pion mis-identification, and 70% to 80% for protons (5 to 20 GeV/c) with 15% pion mis-identification. Below 5 GeV/c the performance is degraded due to track direction uncertainty caused by multiple Coulomb scattering.

Examples of performance and of impact on physics analyses are show in Figs. 18-20. Invariant mass distributions for two tracks attributed to charged pions show a peak at the kaon mass. From Fig. 19, it is seen that the inclusion

of the requirement that both tracks in fact belong to kaons improves the signal to background ratio. Fig. 18 shows the same effect of particle identification on the measured $\Lambda \to \pi^- p$ decays. Analysis of measured data resulted in the hadron fractions shown in Fig. 20, which agree within errors with Monte Carlo predictions (39).

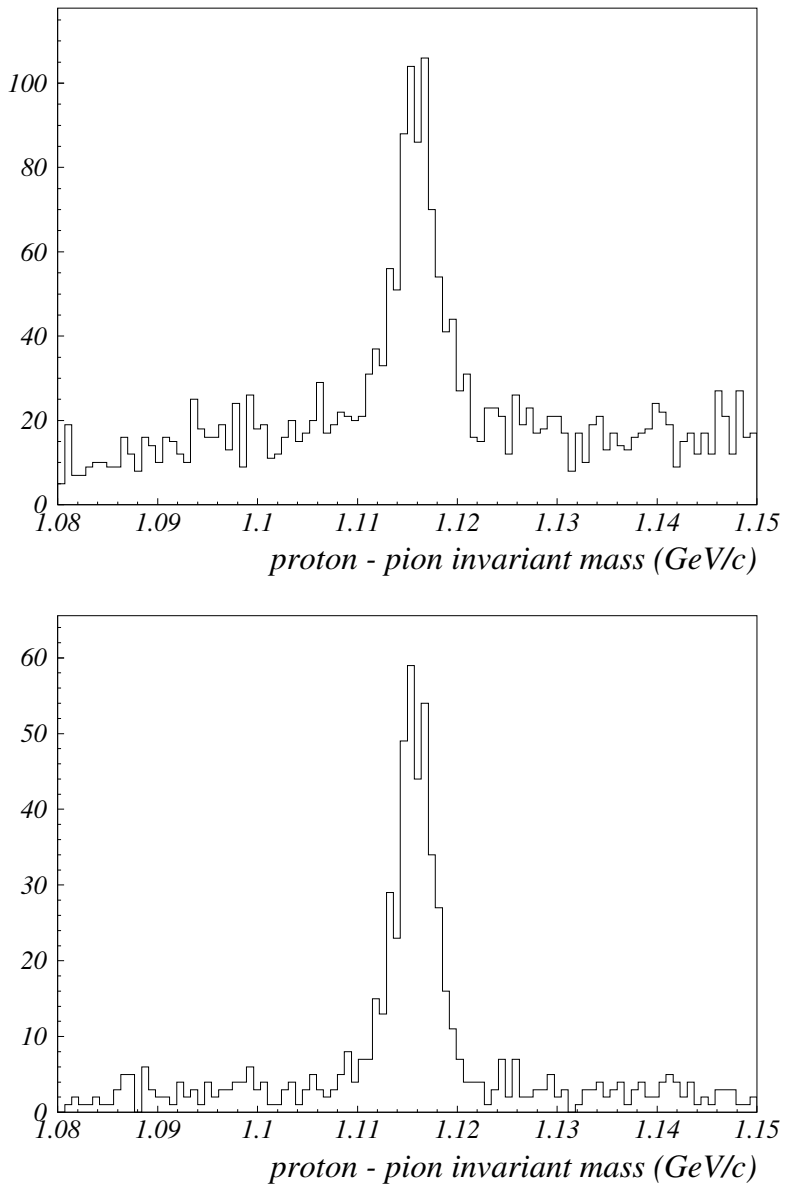

Fig. 18. Improvement of signal to background for invariant mass distribution of $\Lambda \to \pi^- p$: a) no particle identification, b) negative particle was required to be a pion, positive a proton.

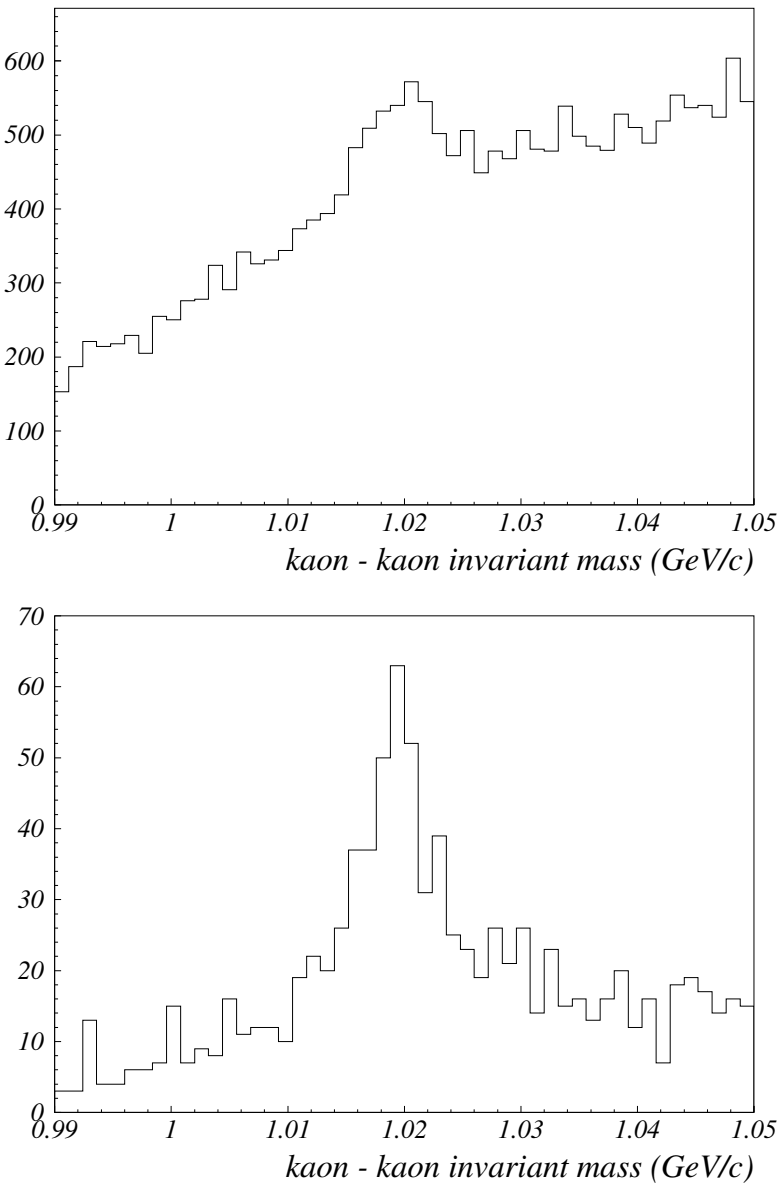

Fig. 19. Improvement of signal to background for invariant mass distribution of $\phi \to K^+K^-$: a) one of the kaons is identified, b) both particles were required to be kaons.

6 RICH as a tracking device

RICH can serve as a stand-alone tracking device (40). This turned out to be very useful in the initial phase of the HERA-B experiment when the main tracking system was not available. From the rings found on the photon detector, track directions are deduced, and matched in the non-bending plane with the track candidates from the silicon vertex detector. From the deflection in the bending plane the momentum of the particle was then determined. The

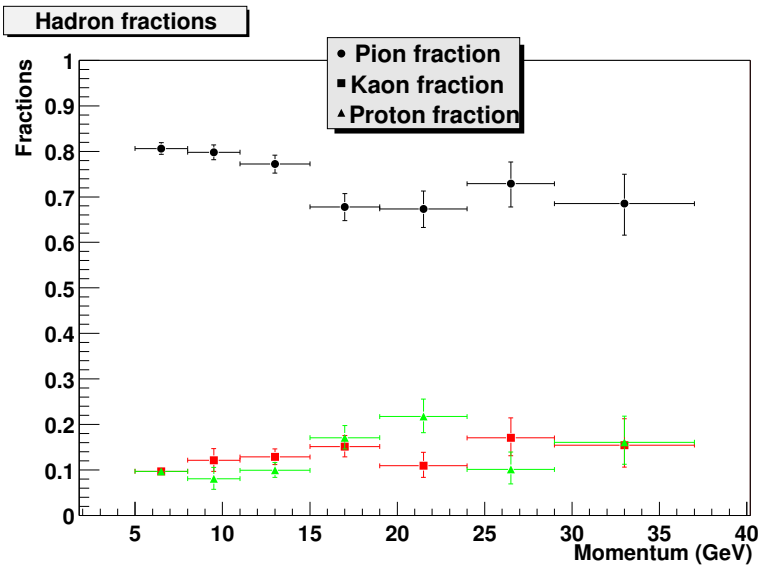

Fig. 20. Measured hadron fraction as a function of particle momentum.

resulting identification capabilities are illustrated in Fig. 21.

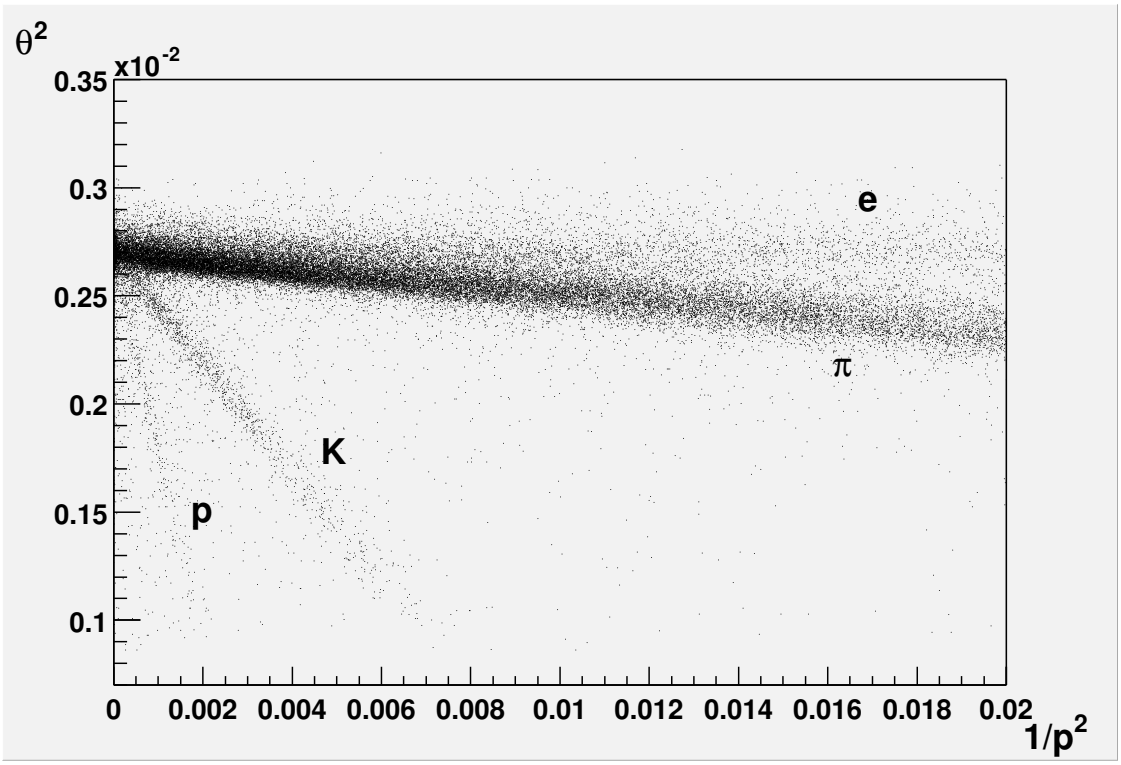

Fig. 21. θ_c^2 versus $1/p^2$ plot in which particles of given mass should lie on a straight line.

7 Summary

We conclude that the HERA-B ring imaging Cherenkov detector behaves as expected in all respects. The detector parameters of $\theta_c = 52$ mrad and 32 photons per $\beta = 1$ particle, $N_0 = 43$ photons/cm and single photon resolutions of $\sigma = 0.7$ mrad for M16 and $\sigma = 1.0$ mrad for M4 PMT's, are in very good agreement with a priori estimates. Results on particle identification of highly populated events also seem to be satisfactory and should meet the requirements. Finally we may add that during the 2 years the detector has been in operation, not the least degradation of operation has been observed.

8 Acknowledgments

References

[1] T. Lohse et al. Proposal for HERA-B, DESY PRC-94/02, May 1994

[2] P. Križan, R. Mankel, D. Ressing, S. Shuvalov, M. Spahn, Nucl. Instr. Meth. in Phys. Res. A351 (1994) 111-131.

[3] J.L. Rosen, Nucl. Instr. Meth. in Phys. Res. A408(1998)191

[4] S. Korpar et al., Nucl. Instr. and Meth. in Phys. Res. **A433** (1999) 128-135

[5] D. Broemmelsiek, *The HERA-B RICH gas system*, HERA-B Note ?????????????

[6] D. Dujmić, K. Reeves, HERA-B RICH Note 97-182, Hamburg 1997

[7] mirror alignment

[8] T. Hamacher et al., Nucl. Instr. and Meth. in Phys. Res. **A371** (1996) 289-294

[9] P. Križan, M. Cindro, V. Cindro, S. Korpar, G. Omahen, A. Stanovnik, M. Starič, Nucl. Instr. and Meth. in Phys. Res. **A364** (1995) 243-252

[10] P. Križan, S. Korpar, M. Starič, A. Stanovnik, M. Cindro, D. Škrk, M. Zavrtanik, T. Hamacher and E. Michel, 1994 IEEE NSS Conference Record, Volume 2 (1995) 985-988

[11] J. Pyrlik at al., Nucl. Instr. and Meth. in Phys. Res. **A414** (1998) 170.

[12] S. Korpar, P. Križan, A. Stanovnik, M. Starič, D. Škrk, IEEE Trans. Nucl. Sci. **46** (1999) 317.
[13] P. Križan, S. Korpar, M. Starič, A. Stanovnik, M. Cindro, D. Škrk, M. Zavrtanik, T. Hamacher, E. Michel, Nucl. Instr. and Meth. in Phys. Res. **371** (1996) 151-154
[14] P. Križan et al., Nucl. Instr. and Meth. in Phys. Res. **A387** (1997) 146-149
[15] Hamamatsu Data Sheets for R5900-M16 and R5900-M4 Photomultipliers
[16] J. McGill, R. Schwitters, HERA-B Note 96-278, DESY, Hamburg (1996); D. Broemmelsiek, Nucl. Instr. and Meth. in Phys. Res. **A433** (1999) 136-142.
[17] R. Eckmann, M. Ispirian, S. Karabekyan, J. McGill, R. Schwitters, HERA-B Note 97-162, DESY, Hamburg (1997)
[18] F.M. Newcomer et al., IEEE Trans. Nucl. Sci. **40?** (1993) 630
[19] asd8 otr board
[20] sharc
[21] H. Calcao et al., IEEE Trans. Nucl. Sci. **46** (1999) 377; H. Calcao et al., HERA-B Note 99-009, DESY, Hamburg (1999)
[22] P. Križan, M. Starič, Nucl. Instr. and Meth. in Phys. Res. **A379** (1996) 124-129
[23] R. Schwitters, HERA-B Note 97-088, DESY, Hamburg (1997); D. Dujmić, R. Schwitters, HERA-B Note 98-052, DESY, Hamburg (1998)
[24] J. Pyrlik and K. Lau, HERA-B Note 97-182, DESY, Hamburg (1997)
[25] P. Križan, S. Korpar, R. Pestotnik, M. Starič, A. Stanovnik, E. Michel, C. Oehser, W. Schmidt-Parzefall, A. Schwarz, T. Hamacher, D. Broemmelsiek, J. Pyrlik, Nucl. Instr. and Meth. in Phys. Res. **A394** (1997) 27-34
[26] V. Cindro, S. Korpar, P. Križan, A. Stanovnik, M. Starič, D. Škrk, Nucl. Instr. and Meth. in Phys. Res. **A337** (1994) 609-612
[27] S. Korpar, R. Pestotnik, P. Križan, IJS Report, IJS-DP-7615, Ljubljana (1997); HERA-B Note 97-079, DESY, Hamburg (1997)
[28] I. Ariño, M. Chmeissani, A. Garcia, Ll. Garrido, R. Miquel, D. Peralta and J. Sieiro, Test of the ASD8 boards, RICH Internal Report (March, 1998)
[29] FieldPoint User Manual, National Instruments Corporation
[30] S. Korpar et al., Proc. of the 2nd Conference on Photodetection, Beaune, France, June 1999, to be published in Nucl. Instr. and Meth. in Phys. Res.
[31] S. Korpar et al., IJS Report, IJS-DP, Ljubljana (1999)
[32] R. Pestotnik, Diploma Thesis, Univerza v Ljubljani, Fakulteta za matematiko in fiziko, Ljubljana (1996).
[33] D. Škrk, Doctoral thesis, Univerza v Ljubljani, Fakulteta za matematiko in fiziko, Ljubljana (1999).
[34] R. Schwitters, HERA-B Note 98-088, DESY, Hamburg (1998); R. Eckmann, D. Dujmić HERA-B Note 00-004, DESY, Hamburg (2000).
[35] D. Dujmić, HERA-B Note 00-016, DESY, Hamburg (2000).

[36] J. Carvalho, HERA-B Note 99-008, Hamburg (1999); M. Ispiryan, S. Ramachandran HERA-B Note 99-184, Hamburg (1999); P. Križan, D. Tement, HERA-B Note 98-157, Hamburg (1998).
[37] I. Ariño, Ll. Garrido, HERA-B Note 99-108, Hamburg (1999).
[38] M. Starič, P. Križan, Nucl. Instr. and Meth. in Phys. Res. **A433** (1999)279.
[39] I. Ariño, Doctoral thesis, University of Barcelona, Barcelona (2001).
[40] R. Schwitters et al., HERA-B Note 00-020, DESY, Hamburg (2000).